Uranium Redox Transformations after U(VI) Coprecipitation with Magnetite Nanoparticles

Pidchenko, I.; Kvashnina, K. O.; Yokosawa, T.; Finck, N.; Schild, D.; Polly, R.; Bohnert, E.; Rossberg, A.; Göttlicher, J.; Dardenne, K.; Rothe, J.; Schäfer, T.; Geckeis, H.; Vitova, T.;

Originally published:

January 2017

Environmental Science & Technology 51(2017)4, 2217-2225

DOI: https://doi.org/10.1021/acs.est.6b04035

Perma-Link to Publication Repository of HZDR:

https://www.hzdr.de/publications/Publ-23834

Uranium Redox Transformations after U(VI) Coprecipitation with Magnetite Nanoparticles

Journal:	*Environmental Science & Technology*
Manuscript ID	es-2016-04035e.R2
Manuscript Type:	Article
Date Submitted by the Author:	03-Jan-2017
Complete List of Authors:	Pidchenko, Ivan; Karlsruhe Institute of Technology, Institute for Nuclear Waste Disposal Kvashnina, Kristina; European Synchrotron Radiation Facility, Yokosawa, Tadahiro; Institute for Nuclear Waste Disposal, Karlsruhe Institute of Technology, Finck, Nicolas; Institute for Nuclear Waste Disposal, Bahl, Sebastian; Karlsruhe Institute of Technology, Institute for Nuclear Waste Disposal Schild, Dieter; Karlsruhe Institute of Technology (KIT), Institute for Nuclear Waste Disposal (INE) Polly, Robert; Research Centre Karlsruhe, Institute for Nuclear Waste Disposal Bohnert, Elke; Karlsruhe Institute of Technology, Institute for Nuclear Waste Disposal Rossberg, Andre; Forschungszentrum Dresden-Rossendorf, Institute of Radiochemistry Göttlicher, Jörg; Forschungszentrum-Karlsruhe, Institute for Synchrotron Radiation Dardenne, Kathy; Institute for Nuclear Waste Disposal, Karlsruhe Institute of Technology Rothe, Jörg; Karlsruhe Institute of Technology, Institut für Nukleare Entsorgung Schäfer, Thorsten; Karlsruhe Institute of Technology, Institute for Nuclear Waste Disposal (INE) Geckeis, Horst; Karlsruhe Institute of Technology (KIT), Institute for nuclear waste disposal (INE) Vitova, Tonya; Karlsruhe Institute of Technology, Institute for Nuclear Waste Disposal ,

Uranium Redox Transformations after U(VI) Coprecipitation with Magnetite Nanoparticles

Ivan Pidchenko,[a] Kristina O Kvashnina,[b,c] Tadahiro Yokosawa,[a] Nicolas Finck,[a] Sebastian Bahl,[a] Dieter Schild,[a] Robert Polly,[a] Elke Bohnert,[a] André Rossberg,[c] Jörg Göttlicher,[d] Kathy Dardenne,[a] Jörg Rothe,[a] Thorsten Schäfer,[a] Horst Geckeis,[a] Tonya Vitova,[a,]*

[a] Karlsruhe Institute of Technology, Institute for Nuclear Waste Disposal (INE), P.O. 3640, D-76021 Karlsruhe, Germany

[b] European Synchrotron Radiation Facility (ESRF), CS40220, 38043 Grenoble Cedex 9, France

[c] Helmholtz-Zentrum Dresden-Rossendorf, Institute of Resource Ecology, P.O. Box 510119, D-01314 Dresden, Germany

[d] Karlsruhe Institute of Technology, Institute for Photon Science and Synchrotron Radiation (IPS), P.O. 3640, D-76021 Karlsruhe, Germany

KEYWORDS

Uranium, redox state, magnetite, HR-XANES, EXAFS.

ABSTRACT

Uranium redox states and speciation in magnetite nanoparticles co-precipitated with U(VI) for uranium loadings varying from 1000 to 10000 ppm are investigated by X-ray absorption spectroscopy (XAS). It is demonstrated that the U M_4 high energy resolution X-ray absorption near edge structure (HR-XANES) method is capable to clearly characterize U(IV), U(V) and U(VI) existing simultaneously in the same sample. The contributions of the three different uranium redox states are quantified with the iterative transformation factor analysis (ITFA) method. U L_3 XAS and transmission electron microscopy (TEM) reveal that initially sorbed U(VI) species recrystallize to non-stoichiometric UO_{2+x} nanoparticles within 147 days when stored under anoxic conditions. These U(IV) species oxidize again when exposed to air. U M_4 HR-XANES data demonstrate strong contribution of U(V) at day 10 and that U(V) remains stable over 142 days under ambient conditions as shown for magnetite nanoparticles containing 1000 ppm U. U L_3 XAS indicates that this U(V) species is protected from oxidation likely incorporated into octahedral magnetite sites. XAS results are supported by density functional theory (DFT) calculations. Further characterization of the samples include powder X-ray diffraction (pXRD), scanning electron microscopy (SEM) and Fe 2p X-ray photoelectron spectroscopy (XPS).

INTRODUCTION

Uranium is the main constituent of spent nuclear fuel (SNF), but it can be also found in high quantities in actinide (An) contaminated sites.[1] Developing the safety case for the safe disposal of radioactive waste requires mechanistic understanding of the interaction of the waste products with repository components. In case of water accessing the waste container, radionuclides will react with the corrosion products, which potentially represent a very relevant reactive barrier retaining pollutants release in the repository near field. Of particular interest is the detailed understanding of An interactions with iron (Fe) oxides, e.g. magnetite (Fe_3O_4) considered as a

corrosion products of Fe based container materials.[2] A number of laboratory studies have been performed to clarify the fate of uranium in such systems. Due to the complex redox processes induced by Fe(II)/Fe(III) species, uranium is often found to exist in a mixture of redox states. Uranium has two main environmentally relevant redox states, U(IV) and U(VI). U(V) is believed to form as an intermediate redox species and exhibits a poorly understood geochemical behavior. The only evidence of U(V) in nature is the uranium mineral wyartite.[3] Whereas U(VI) and U(IV) are usually found, depending on conditions, as a result of microbial and Fe(III)/Fe(II) driven redox processes,[4-10] only a few studies report U(V) as a relevant redox species. In earlier studies U(V) was detected after Fe(II) catalyzed transformation of U(VI)-ferrihydrite to goethite (α-FeO(OH))[11] and in different Fe (oxyhydr)oxides phases where Fe_3O_4 was considered as one of the possible phases to stabilize U(V).[12] Also Nico et al. reported on the possibility of U(V) or U(VI) incorporation into the octahedral position of the α-FeO(OH)/Fe_3O_4 after ferrihydrite remineralization.[13] Later studies attempted to specifically detect U(V) in different Fe systems under controlled conditions with the aim to reconsider the relevance of U(V) for uranium containing (geo)chemical systems.[14-17] In most of the reported investigations, X-ray absorption spectroscopy (XAS) based methods, i.e. U L_3 X-ray absorption near edge structure (XANES) and extended X-ray absorption fine structure (EXAFS) as well as U 4f X-ray photoelectron spectroscopy (XPS) are used to investigate the U speciation and redox states. XANES spectra are sensitive to the U coordination environment and redox states but the spectra are dominated by broad features due to large core-hole lifetime broadening effects.[18] This challenges the characterization and quantification of the different U redox states, especially when U(V) is also present in the material. On the other hand, the XPS technique can successfully quantify mixed U redox states if there is sufficiently high uranium content (> 1000 ppm) in the sample.[12, 14, 16, 19] However a clear identification of U(V) species can be hampered by low signal to noise ratio of

the spectra for low uranium contents. XPS has high surface sensitivity and is performed in ultra-high vacuum, which can lead to potential changes of the samples. To handle these challenges, complementary highly sensitive techniques are needed for thorough characterization of the U redox states in such systems. The high energy resolution XANES (HR-XANES) method at the U $M_{4,5}$ absorption edges was demonstrated to be very valuable for studies related to U redox state analysis in complex uranium systems containing mixed U redox states.[20, 21] The U M_4 HR-XANES experiments need to be performed in He environment comprising the sample, analyzing crystals and detector in order to avoid loss of intensity by scattering and absorption of photons in air. Unlike XPS, vacuum conditions are not necessary. The samples can be investigated in the form of solids, wet pastes, suspensions or liquids. U $M_{4,5}$ HR-XANES takes a great advantage over the conventional U L_3 XANES. Reduced core-hole lifetime broadening results in better-resolved spectral features allowing more precise redox state analysis. Due to the dipole selection rule ($\Delta l = \pm 1$) the electrons are excited with high probability from U $3d_{3/2}$ to U 5f unoccupied states. Therefore the U M_4 HR-XANES technique is also a direct probe of the unoccupied U 5f valence states, which play a significant role in the chemical bonding of the An elements.[20-24]

In the present study we investigated the U redox states and speciation in the final product formed by co-precipitation of U(VI) with Fe_3O_4 for variable U loadings (1000-10000 ppm). The U L_3/M_4 HR-XANES and U L_3 XANES/EXAFS as well as transmission electron microscopy (TEM) are applied. Scanning electron microscopy (SEM), X-ray powder diffraction (pXRD), Fe $2p_{3/2}$ XPS, geochemical calculations and density functional theory (DFT) are used to characterize the U containing Fe_3O_4 samples. The main aim is to verify the presence of U(V) in this system. A long-term study of samples kept under anoxic (up to 480 days) and oxidizing conditions (up to 226 days) was performed to elucidate the stability of the potential U(V) species in the Fe_3O_4 nanoparticles. We demonstrate that the applied U M_4 HR-XANES method is capable of detecting

U(IV), U(V) and U(VI) at relatively low (1000 ppm) total U concentrations being present simultaneously in the same sample. The contributions of the three different U redox states are quantified with the iterative transformation factor analysis (ITFA) method.[25]

MATERIALS AND METHODS

Preparation of the samples. MilliQ-H_2O was used for the preparation of all samples. To remove dissolved O_2 and CO_2 MilliQ-H_2O was bubbled for several hours with Ar outside and then for at least one hour inside an argon (Ar) glovebox. Uranium containing Fe_3O_4 nanoparticles were synthesized by direct precipitation [26-28] inside an Ar glovebox equipped with pH, E_h electrodes and a dropping funnel using the following procedure: to a 50 mL Teflon container the calculated amounts of aqueous $FeCl_3$, $FeCl_2$ and an aliquot of aqueous U(VI)O_2Cl_2 (1000, 3000, 6000 and 10000 ppm U: Um1-Um10 samples) were added followed by dropwise addition of 0.5 M NaOH (Backer, CO_2 free) to pH = 7.5-8.0. The suspension was stirred overnight, pH and E_h values were recorded and pH was adjusted if necessary by adding 0.1 M NaOH. All samples were then stored in the form of suspension in the Ar glovebox. The UO_2 (several μm particle size), U_4O_9 (used from[20, 29]) and 3000 ppm U(VI) adsorbed onto maghemite (γ-Fe_2O_3, spectra are named Umh) serve as reference compounds. The γ-Fe_2O_3 was prepared by heating freeze-dried magnetite nanoparticles at 200 °C during 2 hours in air.[30] 3000 ppm U as U(VI)O_2Cl_2 was then adsorbed on the γ-Fe_2O_3. More than 99 % of U(VI) was adsorbed after 50 days as determined with inductively coupled plasma mass-spectrometry (ICP-MS). Experimental details for U, Fe and salt concentrations as well as pH, E_h measurements are given in Table S1.

For the U L_3/M_4 HR-XANES experiments, solids were separated from supernatant using a Nd magnet. The supernatant was decanted and the solids were used in the form of a wet paste. All samples were prepared in an Ar glovebox at 1-2 ppm O_2 level and less than 1 ppm CO_2. An inert gas Plexiglas sample holder comprising a double containment (two separated 10 μm

polypropylene films) has been designed and used for the spectroscopic measurements. To avoid contact of the samples with air they were transported one day prior to the experiments in a gas tight aluminum cylinder filled with Ar and opened very shortly prior to the experiments.

For the U L_3 XAS experiments, subsamples Um1-Um10 from the same batch were separated using a Nd magnet after 147 days of ageing in the Ar glovebox. After these experiments the Um1 sample was placed in a non-hermetically closed plastic vial and kept under ambient, aerobic conditions (Um1a sample). The Um1a sample was investigated with the U M_4 HR-XANES (142 days in air, total 289 days) and with the U L_3 XAS (XANES and EXAFS) techniques (226 days in air, total 373 days).

X-ray absorption spectroscopy (XAS). U L_3/M_4 HR-XANES experiments were performed at the ID26 beamline, ESRF, Grenoble, France[31] (Um1-Um10) and at the INE-Beamline, ANKA, Karlsruhe, Germany[22] (Um1a) with Johann type X-ray emission spectrometers.[24, 32, 33] The U L_3 XAS (XANES and EXAFS) experiments were performed in fluorescence mode using a five element Ge solid state fluorescence detector (Canberra) at the INE-Beamline. The ATHENA and ARTEMIS program parts of the IFFEFIT program package were used for data reduction and analyses of the EXAFS spectra.[34, 35] Details on the experiments, the quantitative U oxidation states analyses of the U M_4 HR-XANES spectra with the ITFA method for the 10 day aged samples and the EXAFS analyses are given in the Supporting Information (SI).

Additional characterization methods. High resolution-TEM (HR-TEM) and SEM images were recorded with a FEI Tecnai G2 F20 X-TWIN instrument operated at 200 kV and a FEI Quanta 650 FEG ESEM, respectively. pXRD patterns were measured with laboratory based Bruker AXS D8 powder diffractometer and at the SUL-X-Beamline (ANKA, Karlsruhe, Germany) (SI).[36] The FIT2D and DIFFRAC.EVA V3.1 programs were used to analyze the data.[37]

DFT calculations. The experiments are supported by DFT calculations utilizing plane-wave basis sets with periodic boundary conditions as implemented in the Vienna Ab initio Simulation Package (VASP).[38-44] Further details are given in SI.

Details on the thermodynamic calculations and the XPS experiments are reported in SI. Table S2 comprises the description of the studied samples and the applied characterization techniques.

RESULTS AND DISCUSSION

Characterization of the Fe_3O_4 nanoparticles. The formation of the Fe_3O_4 nanoparticles can be described with reaction 1,

$$Fe^{2+} + 2Fe^{3+} + 8OH^- \rightarrow Fe_3O_4 \downarrow + 4H_2O \quad (1)$$

Measured E_h-pH values for samples containing 1000 ppm U (Um1) and 10000 ppm U (Um10) are located inside the stability field of Fe_3O_4 according to the Fe Pourbaix diagram (Figure S1A); redox conditions of the samples comprising 3000 ppm U (Um3) and 6000 ppm U (Um6) are placed at the border of Fe_3O_4 – FeO(OH)(cr) (goethite) stability fields.[45] E_h-pH conditions are such (E_h = -210 – -390 mV; pH = 7.5-8.0) that subsequent reduction of U(VI) to U(IV) would be expected according to the U Pourbaix diagrams (Figures S1B, C). SEM images (Figure S2) and powder XRD (pXRD) patterns (Figure S3) reveal that crystalline Fe_3O_4 nanoparticles with octahedral shape and a size of 15-40 nm are formed. Energy dispersive X-ray analysis (EDX) does not reveal segregated uranium precipitates. No goethite or any other Fe containing crystalline phases are found. The Fe(II) content is slightly below that of stoichiometric Fe_3O_4 ($Fe(II)/Fe_{TOT} = 0.33$) at $Fe(II)/Fe_{TOT} = 0.28 \pm 3$ % for all samples (Um1-Um10) aged for 310 days as indicated by the reduced intensity of the Fe(II) $2p_{3/2}$ peak of the Fe 2p XPS spectra (Figure S4). There is no clear trend in the level of Fe(II) oxidation as a function of the U(VI)

concentration. In view of the low U/Fe mass ratios (0.0014-0.014), this is indeed not to be expected.

Redox states of U in the Fe_3O_4 nanoparticles aged for 10 days. We characterized the U redox state in the Um1-Um10 samples aged in inert atmosphere for 10 days with the U L_3 and M_4 HR-XANES spectroscopy techniques. The U L_3 and M_4 HR-XANES spectra of the Um1-Um10 samples are depicted in Figures 1A and 1B, respectively.

The X-ray absorption spectra typically shift to higher energies by increasing the U redox state due to the reduced screening of the $2p_{3/2}$ (L_3)/$3d_{3/2}$ (M_4) core-hole by the decreased electronic charge density on the U atoms. Smaller energy shifts of about ± 0.5 eV can be induced by variations of the electronegativity of the bonding partner, changes in symmetry, short and long range atomic order etc., for the same U redox state as suggested by U L_3 XANES studies.[46, 47] One exception of the general trend are the U L_3 XANES spectra of U(V) and U(VI) forming short (< 1.9 Å) axial bonds with two O atoms (UO_2^+/UO_2^{2+}, U(V)/U(VI)-yl); the maxima of the most intense absorption resonance (white line, WL) of the U(V)-yl and UO_2 spectra have similar energy positions.[19] The WL of the U(VI)-yl spectrum is only slightly shifted to higher energy and it can potentially have the same energy position as e.g. U(V) species with more symmetric coordination environments associated with loss of short uranyl bonds, i.e. uranate type of U(V) species. This effect is induced by the large electronic density in the vicinity of U due to the strong covalent bond of U(V)/U(VI) with the two axial O atoms. Such anomalous behavior is not observed for U $M_{4,5}$ HR-XANES spectra. Energy shifts within a range of ± 0.1 eV can be caused by differences in short and long range atomic order around the absorbing atom as for example observed for different UO_3 phases, but the spectra shift to higher energies for higher U oxidation states.[21, 48] For example the energy shift between UO_2 and U(V)-yl ($[U(V)O_2(CO_3)_3]^{5-}$) is ~1.2

eV, whereas between U(V)-yl and U(VI)-yl ($[U(V)O_2(CO_3)_3]^{5-}$and $[U(VI)O_2(CO_3)_3]^{4-}$) is ~1.0 eV.[49]

The WL of the U L_3 HR-XANES spectrum of the Um10 sample is located at similar energy position as the WL of the spectrum of Umh. U has oxidation state U(VI) in the Umh sample. In addition, the feature marked with line c clearly visible in the U L_3 HR-XANES Umh and Um10 spectra (Figure 1A) is characteristic for the $U(VI)O_2^{2+}$/$U(V)O_2^{+}$ entity. These results suggest predominant U(VI)-yl contribution in the Um10 sample. The absorption resonance marked with line c becomes less intense in the spectra of the Um6-Um3 samples and it diminishes in the spectrum of the Um1 sample. These spectra suggest that the Um1 sample if at all contains low amount of uranyl species. In addition, the WL and the post edge absorption resonance marked with line c´ become broader and asymmetric from the Um10 to the Um1 spectrum. Such asymmetric WLs have been previously described as being characteristic for uranate type of U(V)/U(VI) species.[19, 46, 50, 51] However it can not be excluded that this U species dominant in the Um1 sample has redox state (IV). The local symmetry of these U(V)/U(IV) species should be rather different compared to the U(V)/U(IV) in U_4O_9 since there is no resemblance between the Um1 and the U_4O_9 spectra. It is clear that the U L_3 HR-XANES spectra are more sensitive to small structural and oxidation states changes compared to the conventional U L_3 XANES.[18, 52] But the method is still limited by large core-hole lifetime broadening effects and does not allow to reliably identify and quantify the U(IV), U(V) and U(VI) anticipated to be simultaneously present in the samples.

Additional information on the U redox states is obtained by applying the U M_4 HR-XANES method. Figure 1B depicts the U M_4 HR-XANES spectra of the Um1-Um10 samples and UO_2, U_4O_9 as well as Umh for comparison. U_4O_9 contains U(IV) and U(V) visible by the two main peaks separated by ~1 eV.[20] These spectral features are named d and e in the U M_4 HR-XANES

spectrum of U_4O_9 (Figure 1B). The main absorption peak f of the Umh spectrum is shifted by ~ 0.4 eV to higher energies as compared to peak e and it is assigned to U(VI). Spectral features f' and f'' are also typical for U(VI)-yl ions with short (~1.77-1.91 Å) trans-dioxo bonds.[23, 48, 53] These features exist for U(V)-yl species but are considerably shifted (f' ~0.6 and f'' ~2.5 eV) towards the main peak.[49]

Much more clear compared to the U L_3 HR-XANES, the U M_4 HR-XANES spectrum obtained for the Um1 sample demonstrates major contributions of U(V) (peak e) and minor fraction of U(IV) (peak d) (Figure 1B). It is also evident that the intensity of feature d increases while moving from the Um10 to the Um1 spectrum, the energy position of feature e shifts to lower energies and features f' and f'' lose intensity. These spectral changes imply that the relative contribution of U(VI) decreases, whereas the U(IV) content rises going from 10000 ppm U (Um10) to 1000 ppm U (Um1) in the samples (Figure 1B).

Quantification of the U redox states. We performed quantitative analysis of the U M_4 HR-XANES spectra by the ITFA method.[25] ITFA is used to decompose the spectral mixtures into the spectra and the fractions of the components (Figure S5). The experimental spectra can be suffieciently reproduced (Figure S5A) by using linear combinations of the three ITFA-extracted component spectra (Figure S5B), so that the residual is similar to the expected experimental error. Only the first three eigenvectors show a signal while the eigenvectors 4, 5 and 6 do not contribute to the data (Figure S5C), hence only three components are necessary to describe the variations in the spectral mixtures. The extracted component spectra corespond to the U(IV), U(V) and U(VI) redox states. The analysis shows that the Um1 and Um10 samples contain 19 % U(IV), 81 % U(V) and 0.7 % U(IV), 62.3 % U(V), 37 % U(VI), respectively (Table S3). The U M_4 HR-XANES technique and the ITFA approach are clearly capable of detecting and

quantifying the three different redox states: U(IV), U(V) and U(VI), being present simultaneously in the same sample.

Redox states and local atomic environment of U in the Fe_3O_4 nanoparticles aged for 147 days. We performed U L_3 XAS (XANES and EXAFS) studies for the magnetite suspensions containing U stored for 147 days in anoxic conditions. For technical reasons, the redox states of U in the Um1, Um3, Um6 and Um10 samples could not be analyzed with the U M_4 HR-XANES method 147 days after the preparation of the samples.

The U L_3 XANES spectra of the Um10-Um1 samples are depicted in Figure 2A. The energy positions of the WLs and the general shapes of the spectra of the Um10 sample and UO_2 are very similar. We conclude that the initial U(VI)-yl has reduced mainly to U(IV) in the Um10 sample. The spectra of the Um10-Um1 samples exhibit a trend and are shifted up to ~1.5 eV to higher energies compared to UO_2 going from the Um10 to the Um1 sample (lines a and b in Figure 2A). The WL becomes broader and the post-edge absorption resonance at ~17218 eV transforms from a single asymmetric (c') to a broad peak shifted to higher energies observed also for the U L_3 HR-XANES spectra of the 10 days aged samples (Figure 1A). We obtain additional insights from the comparison of the conventional U L_3 XANES spectra measured for the Um1 samples aged for 10 and 147 days (Figure S6). The U L_3 XANES for the Um1 sample aged for 147 days is shifted ~2,5 eV to lower energies compared to the spectrum of the sample aged for 10 days, which is an evidence for higher U(IV) content (Figure S6). This result implies that reduction of U(V) to U(IV) has continued for the Um1 sample 10 days after its preparation. We assume that the higher oxidation state of U in the Um1 sample aged for 147 days is the U(V) species found for the 10 days aged Um1 sample. U(VI) was not found for the 10 day aged Um1 sample by the ITFA U M_4 edge HR-XANES analyses and since the Um1-Um10 samples were handled in the same way, i.e.

anoxic and reducing conditions, it is likely that U has reduced in all samples. Therefore the observed energy shift can not be explained with major U(IV) and minor U(VI) contributions. Alternatively, if the U has completely reduced to U(IV), this can be U(IV) in different coordination environment compared to the U(IV) typical for the Um10 sample. However published spectra for U(IV) in different coordination environments show no significant differences in the energy positions of the WL maxima of the U L_3 XANES spectra.[54]

The FT-EXAFS spectra and their best fits for the Um1, Um3, Um6 and Um10 samples after 147 days ageing are depicted in Figure 2B (see also Figures S7-9). The first coordination sphere of U is best modeled with three U-O distances (R). R(U-O1) = 1.69(2)-1.73(2) Å is an untypically short bond length for U(VI)-O_{axial}, which has been previously observed and controversially discussed.[55, 56] Particularly Conradson et al. proposed that these short U-O distances are characteristic for U(VI) in a series of UO_{2+x} compounds.[55] The structural parameters obtained from the fit to the FT-EXAFS are very similar with and without modeling these peaks; we chose not to consider these very short U-O distances (< 1.75 Å) in our structural model since they can be also part of a background signal. More detailed discussion on their potential structural meaning is not in the scope of our study.

Due to the low signal to noise ratio of the EXAFS data particularly for the Um1 and Um1a samples we have performed and report fits to the spectra for k range until 9.5 $Å^{-1}$ (Figure S10). The main U-O2 distance obtained from the fits to the data continuously decrease from 2.26(1) Å to 2.18(2) Å within the Um10-Um1 series, whereas the U-O3 distance remains within the range R = 2.41(1) Å (Table S4, Figure S11). The coordination numbers (N) vary: N(U-O1) = 0.2(1)-0.4(2), N(U-O2) = 2.2(2)-3.0(3) and N(U-O3) = 3.2(3)-1.8(2) (Table S4, Figure S11). The observation that the first O coordination sphere of U splits into two dominant peaks was reported for UO_{2+x} (x = 0-0.2) compounds where the split became more pronounced for large x.[55] We

therefore might assume that U in our samples exists mainly as non-stoichiometric UO_{2+x} containing mixed U redox states. However, the trend for these two main U-O distances is reversed compared to our EXAFS results since R-O2 and R-O3 grow as a function of the increasing non-stoichiometric oxygen in UO_{2+x} with R(U-O2) = 2.22-2.26 Å and R(U-O3) = 2.36-2.42 Å.[55] This can be explained by the presence of a second U site in our samples in addition to U(IV)/U(V)/U(VI) constituents of UO_{2+x} particles. This U species becomes more relevant at low uranium concentration (1000 ppm U), which agrees with the results from the U L_3 XANES data. The R(U-O2) = 2.18 Å for the Um1 sample is within the range R = 2.05-2.20 Å reported in the literature as typical for U(V) compounds.[12] These EXAFS results do not contradict to the assumption that the U(V) found in the Um1 10 days aged sample is at least partially preserved. This potential U(V) species is likely coordinated by Fe as the best fits to the FT-EXAFS spectra reveal. This is based on the finding that coordination of U to Fe atoms is more prominent for the Um1 compared to the Um10 sample. Two U-Fe interatomic distances are resolved: N(U-Fe1) = 0.6(3), R(U-Fe1) = 3.13(3) Å in Um10 and N(U-Fe1) = 4.5(17), R(U-Fe1) = 3.19(1) Å in Um1. A U-Fe2 shell with a minor contribution (N = 0.5(3)-1.0(8)) is modeled too (Table S4). Somewhat longer R(U-Fe) (+ 0.04 Å) and N(U-Fe) = 6 (fixed) values have been reported for U incorporated into Fe octahedral sites.[15]

We still need to consider possible U(IV) species incorporated in Fe_3O_4. Kerisit et al. calculated similar R(U-Fe1) = 3.18 Å for U(V) and R(U-Fe1) = 3.19 Å for U(IV) incorporated in Fe_3O_4. The R(U-O) = 2.10 Å is much shorter for U(V) compared to R(U-O) = 2.23 Å for U(IV) and closer to the experimental results for the oxidized Um1a sample with R(U-O) = 2.13 Å (cf. section Redox states of U in the Fe_3O_4 nanoparticles exposed to air).[57] As we discuss below the U(V) species in Um1 and Um1a are very similar but there is less interference with near U-O shells for the Um1a compared to the Um1 samples since UO_2/UO_{2+x} is oxidized to form U(VI)-yl

in the former. To the best of our knowledge there is no report for U(IV) incorporated in octahedral Fe_3O_4 sites. Based on these evidences, we conclude that U(V) not U(IV) is more likely to be incorporated in the structure of Fe_3O_4. (cf. DFT calculations).

In contrast, UO_{2+x} species dominate in the Um10 sample. The R(U-O2) = 2.26 Å and R(U-O3) = 2.41 Å obtained from the EXAFS analyses for this sample are very similar to the reported values for $UO_{2.17}$-$UO_{2.20}$.[55] The authors describe strong variations of the R(U-O) in the first coordination sphere as a function of x in UO_{2+x}. In our system R(U-O2) changes as a function of the U concentration due to the increasing contribution of the second U(V) species, whereas R(U-O3) remains constant. Hence it is apparent that the proposed UO_{2+x} has similar stoichiometry in all samples. Presence of UO_{2+x} in the Um1-Um10 samples is also demonstrated by the intense peak at about 3.84 Å characteristic for the scattering of the photoelectron from U atoms in the second U coordination sphere. The N(U-U1) vary within 5.8(8)-2.4(8) in the Um10-Um1 series. The coordination numbers are significantly smaller than those found for bulk UO_2: N(U-O)= 8 and N(U-U) = 12. This can be due to structural disorder and the large contribution of U surface atoms in the small nanoparticles, resulting in destructive interference and thus in decreasing amplitudes of the EXAFS.[41, 48] However, it can be also explained by the fraction of incorporated U atoms versus UO_{2+x} nanoparticles. There is a distinct trend in the coordination numbers. The N(U-U1) and N(U-O3) decrease, whereas N(U-Fe1) increases going from Um10 to Um1 (Figure S11). We assume that minor redox changes have occurred for the Um1 sample since the characteristic for UO_{2+x}: N(U-O3) = 1.8(2), N(U-U1) = 2.4(8) and for U incorporated in magnetite: N(U-Fe1) = 4.5(17) correspond to about 19 % of U(IV) and 81 % U(V) found also from the quantitative analyses of the U M_4 HR-XANES data for 10 days aging of the samples. Correspondingly, if the about 37 % U(VI) found for the Um10 sample aged for 10 days has reduced to U(IV) and if we take into account the initial 0.7 % U(IV), the coordination numbers will be similar to those

reported for the 147 day aged Um10 sample: N(U-O3) = 3.2, N(U-U1) = 5.8. The coordination numbers obtained from EXAFS analyses can have uncertainties up to 30 %. But since we compare them in a system with systematic structural variations, the magnitude of the uncertainty is significantly reduced.

TEM analyses clearly confirm our interpretation of the EXAFS data since it detects crystalline UO_2 nanoparticles with size of about 4-5 nm (Figure 3A) possibly grown on the surface of the Fe_3O_4 particles (Figure 3B) with lattice parameters very close to stoichiometric UO_2. Due to the relatively large uncertainty for the obtained lattice parameter (a = 0.271 ± 0.004 nm) it is not possible to distinguish between UO_2 and UO_{2+x}. Considering also the EXAFS results, we conclude that they are both likely.

It is useful to discuss potential formation of U(IV), U(V) or U(VI) inner sphere complexes sorbed on Fe_3O_4. Indeed U(IV) inner-sphere complexes stable within a few months have been reported to form on Fe_3O_4 surfaces; the R(U-O) is elongated and the N(U-O) is higher (R(U-O) = 2.42 Å, N(U-O) = 9) compared to UO_2 (R(U-O) = 2.35 Å, N(U-O) = 8).[54] For this U(IV) sorbed species almost no U-U coordination is found similarly to U(IV) sorbed onto a Ti substituted Fe_3O_4. Moreover R(U-Fe) = 3.56-3.59 Å are reported, which are significantly longer compared to the distances found in our system, R(U-Fe1) = 3.13-3.19 Å. Indeed the R(U-O) = 2.42 Å is comparable to the R(U-O3) for our Um10-Um3 samples (Table S4). However, our EXAFS analyses report higher N(U-U) for the Um10 sample, N(U-U1) = 5.8, which is in a good agreement with the crystalline UO_2/UO_{2+x} particles found by TEM. Latta et al. showed that UO_2 nanoparticles, are formed for high U surface coverage for samples aged for several months under anoxic conditions.[54] They found systematic change of the only one U-O and the U-U distances as a function of the U concentration not observed for our system. We conclude that

formation of crystalline UO_2/UO_{2+x} nanoparticles is much more probable compared to sorbed U(IV) species.

The possibility for U(V) stabilized on Fe(II) containing mineral surfaces as an inner sphere complex has been discussed;[58] however no exact structural model was described. The stabilization of U(V) seems to be more likely in the form of mixed U(V)-U(VI) oxyhydroxide.[59] For this compound two very long $R(U\text{-}O_{axial})$ = 2.41-2.44 Å and four shorter equatorial O ligands $R(U\text{-}O_{equat})$ = 2.06 Å are found. Our EXAFS results do not report U-O bond distances, which correspond to the distance obtained for the equatorial ligands therefore this model does not seem to be appropriate.

U(VI) complexes sorbed on Fe oxides have two axial O atoms at about ~1.79 Å, six equatorial O atoms at about ~2.38 Å and N(U-Fe) ~2(5), R(U-Fe) > 3 Å.[60] Since we find N(U-Fe) ~4.5 and no strong evidence for stabilization of uranyl, we conclude that the formation of U(VI)-yl is not likely.

DFT calculations. The aim of the calculations is to verify if it is energetically favorable to incorporate U(V) into a magnetite site. In the DFT calculations with periodic boundary conditions we used a 2 × 2 × 2 super cell of magnetite and replaced one Fe^{2+} and one Fe^{3+} by U^{5+} and one vacancy ($Fe^{2+}+Fe^{3+}\rightarrow U^{5+}+\square$). The Fe^{2+} and Fe^{3+} were chosen to be close to each other, hence the presence of the vacancy allows the substitution of Fe by U to relax more easily. Since U(V) is an open shell system we carefully monitored the occupation of the 5f orbitals and the orientation of the spin of this electron. U(V) can be incorporated into a Fe^{2+} or Fe^{3+} octahedral site, since both cases are energetically very close to each other (cf. Figure 3C). We found that the orientation of the spin is important. The spin of the 5f electron points in the opposite direction compared to the spins of the two replaced Fe ions. For the R(U-O2) and the R(U-Fe1) we calculated theoretical values of 2.15(3) Å and 3.18(4) Å, respectively, which are in excellent

agreement with the experimental results, R(U-O2) = 2.18 Å and R(U-Fe1) = 3.18 Å, respectively (Table S4).

Redox states of U in the Fe_3O_4 nanoparticles exposed to air. In order to verify possible existence of U(V) in octahedral Fe_3O_4 environment the Um1 sample aged for 147 days in Ar atmosphere was exposed for 142 days (U M_4 HR-XANES) and for additional 84 days (U L_3 XANES and EXAFS) to air. The U M_4 HR-XANES spectrum of Um1a (142 days in air) is depicted in Figure 4A. The shoulder characteristic for U(IV) is not visible, whereas features f' and f'' typical for U(VI)-yl appear in the spectrum. The main peak maximum has an energy position very similar to the spectrum of the Um1 sample aged for 10 days in Ar, which confirms that the main redox state of U is U(V) (Figure 4A). After exposing this Um1a sample to additional 84 days in air U L_3 XAS (XANES and EXAFS) spectra were recorded. The U L_3 XANES is not as informative as the U M_4 HR-XANES but it can help to verify if any substantial changes of the U oxidation state has taken place. The energy positions of the WL and the post edge absorption resonance of the U L_3 XANES spectra of the Um1 aged for 10 days and the Um1a (226 days in air) samples are comparable, which is an indication that the majority of the U(V) remains stable in the Um1a sample exposed to air for additional 84 days (Figure S6).
The FT-EXAFS spectra of the Um1a (226 days in air) and the Um1 (aged for 147 days in Ar) samples are compared in Figure 4B. It is apparent that the peaks characteristic for U coordination to O and Fe are preserved: N(U-O2) = 2.8(2), R(U-O2) = 2.13(1) Å; N(U-O3) = 0.8(2), R(U-O3) = 2.36(2) Å and N(U-Fe1) = 6.2(17), R(U-Fe1) = 3.19(1) Å, whereas the peak describing the coordination to U is absent in the FT-EXAFS Um1a spectrum. The U(IV) in the UO_{2+x} particles is likely oxidized to $U(VI)O_2^{2+}$ as suggested from the R(U-O1) = 1.78(1) Å with N(U-O1) = 0.7(1). The disappearance of the peak characteristic for U at about 3.84 Å can be explained by increased disorder during the partial oxidation of U leading to destructive interference of the

scattered photoelectron waves. Alternatively, the U-U coordination can disappear due to a phase transformation to a U(VI) phase, which does not contain U atoms at this distance. We did not find crystalline U containing phases for the Um1a sample by applying pXRD. The relatively long-term stability (142 days) of U(V) upon exposure to air (Um1a) can be explained by its incorporation into the octahedral sites of Fe_3O_4, where it is possibly protected against oxidation.

U redox transformation model. We propose the conceptual model presented in the abstract graphics. More than 90 % of initially added U(VI) has adsorbed, most likely on ferrihydrite [16, 61] which is formed in the first stage after Fe(III) titration by NaOH solution and later recrystallizes to Fe_3O_4 through intermediate Fe (oxyhydr)oxide phases.[27]

Part of U(VI) stays adsorbed onto the Fe_3O_4 after 10 days of ageing time. We suppose that the U(V) species have incorporated into the structure of Fe_3O_4 during the formation of the nanoparticles as suggested by the more symmetric local coordination environment compared to uranyl and coordination to Fe. Minor formation of U(IV) in the form of UO_2/UO_{2+x} or sorbed onto the surface is also possible.

After 147 days the U(VI) species have undergone phase transformation and reduction to UO_2/UO_{2+x}, whereas major part of the incorporated U(V) species is preserved. When exposed to air for more than 142 days U(IV) oxidizes to U(VI), whereas U(V) remains stabilized incorporated into octahedral sites of Fe_3O_4.

The experimental results illustrate that reduction of U(VI) to U(IV) is likely to take place, expected from geochemical calculations, with apparently the highest U(IV) fraction for the sample with the highest uranium content (10000 ppm). The relative fractions of U(IV), U(V) and U(VI) depend on the initial uranium concentration while the kinetics of the uranium redox processes depends on the pH/redox conditions, $Fe(II)/Fe_{TOT}$ ratio as well as the rate of electron transfer between Fe^{2+} and Fe^{3+} ions in the octahedral sublattice.

The present study demonstrates the capability of U M_4 HR-XANES to clearly distinguish three different U redox states, U(IV), U(V) and U(VI), in one sample and shows also the potential to identify redox states for other actinides. Previously, U(V) was observed in different Fe(III) (oxyhydr)oxides.[11-17] Our observation that U(V) can also be stabilized in Fe_3O_4, which is a mixed Fe(II)/Fe(III) phase, suggests that the U(V) stabilization range can be extended to more reducing conditions. When exposed to air, apparently, the surrounding mineral matrix is able to protect U(V) against oxidation. This might explain the observation of significant U(V) fractions in redox systems where predominantly U(IV) or U(VI) would be expected considering thermodynamic calculations. This shows that there is a lack of kinetical data to reliably describe and predict uranium speciation in such complex systems. Further studies of U interaction with Fe phases with varying Fe(II)/Fe(III) ratios will be of interest extending the redox/pH conditions where U(V) can be stabilized.

Notably for the discussion on the relevance of U(V) species in the environment, U $M_{4,5}$ HR-XANES combined with EXAFS and other techniques appears to be a powerful spectroscopic tool, which is able to provide distinct answers. Another aspect of future studies is to analyze systems with lower, environmentally relevant U concentrations, e.g. < 100 ppm U, and to investigate a representative U-Fe containing natural system with a varying set of geochemical conditions leading to different U redox and immobilization/mobilization scenarios.

FIGURES

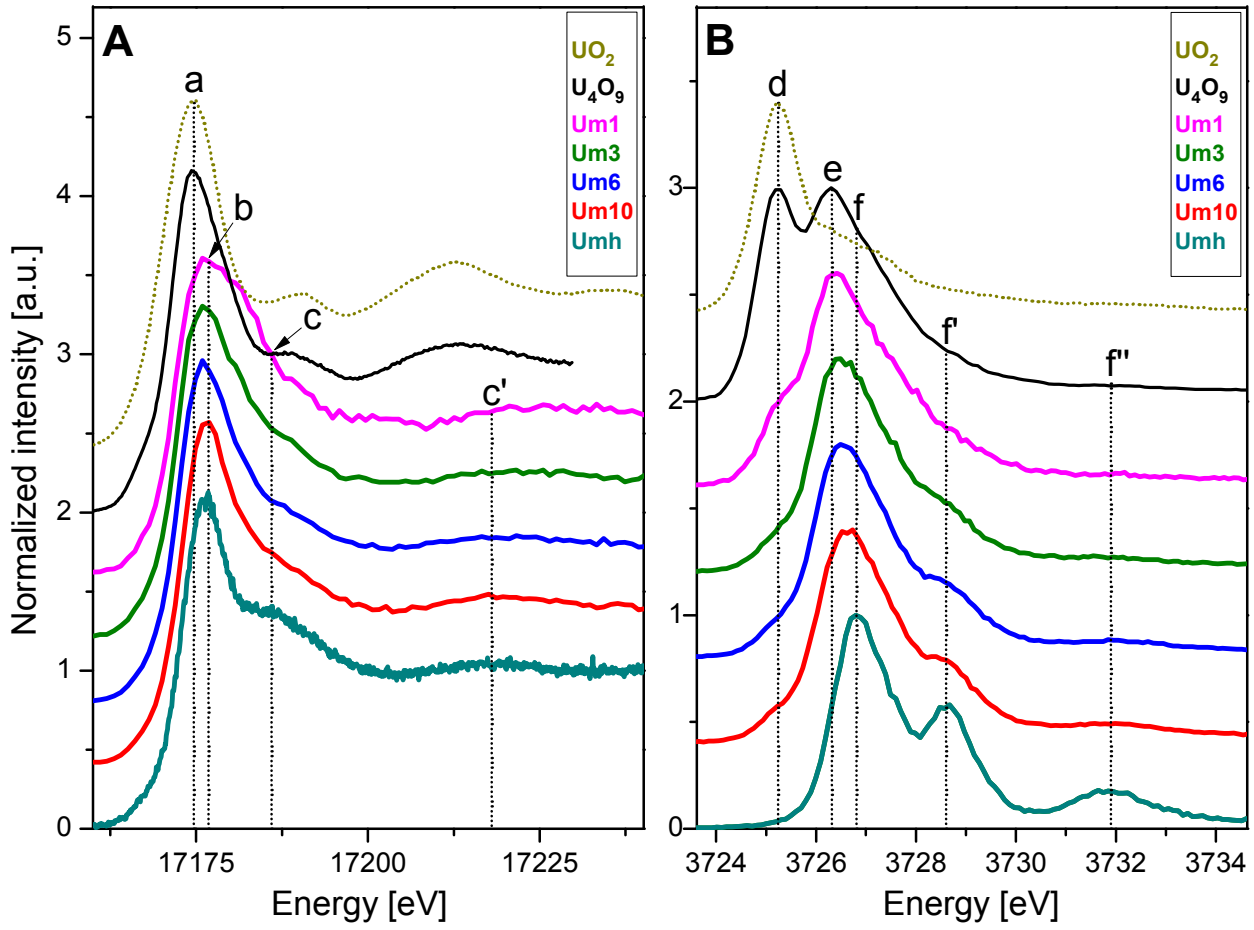

Figure 1. From bottom to top: U L_3 HR-XANES (A) and U M_4 HR-XANES (B) spectra of the Umh reference (U(VI) sorbed on maghemite for 55 days) and the Um10, Um6, Um3, Um1 samples aged for 10 days in anoxic conditions as well as the U_4O_9 and UO_2 references.

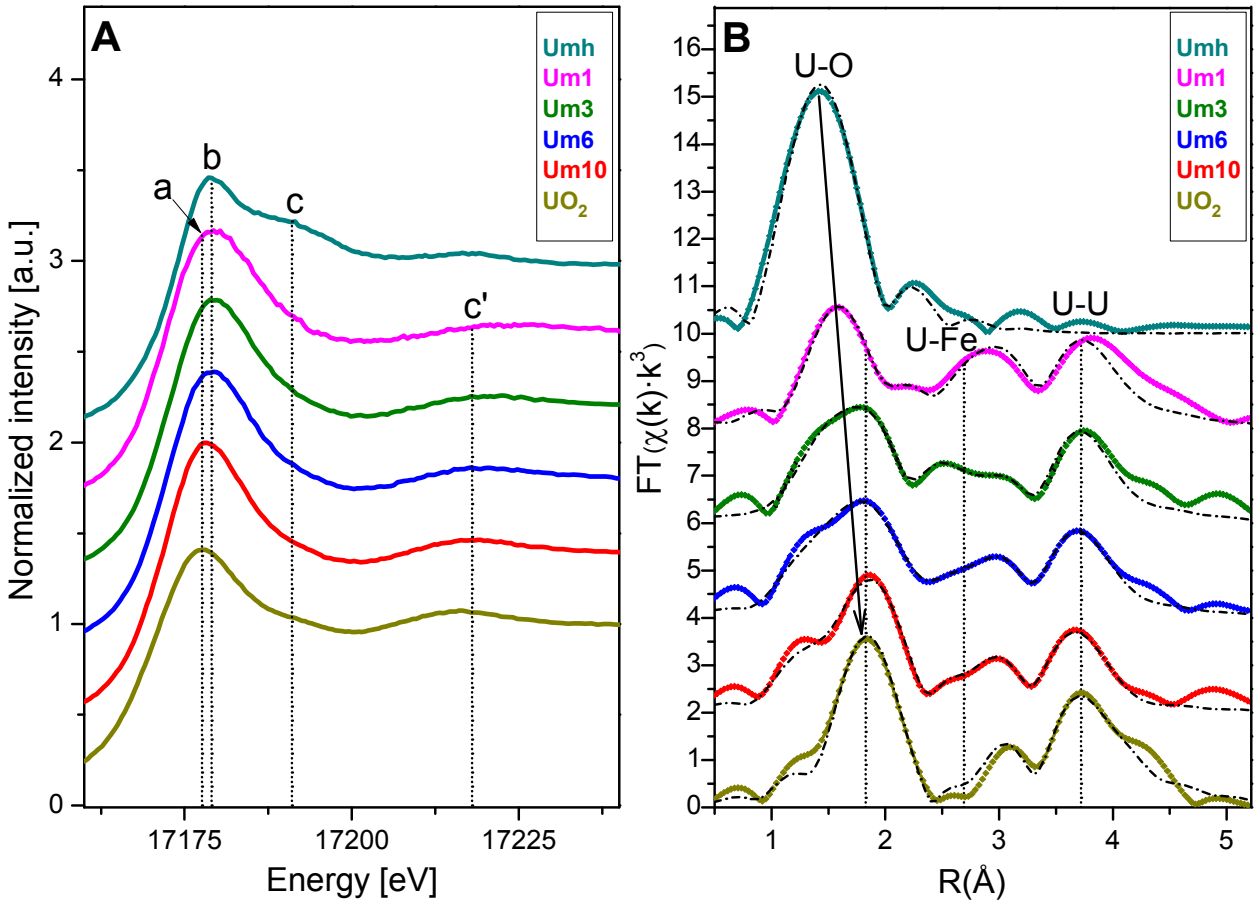

Figure 2. From bottom to top: U L_3 XANES (A) and FT-EXAFS spectra in R space (B) of the UO_2 reference and the Um10, Um6, Um3, Um1 samples aged for 147 days in anoxic conditions as well as the Umh reference (U(VI) sorbed on maghemite for 330 days). The FT-EXAFS and the best fit to the data are given in colored rhombs and in dash dot, respectively.

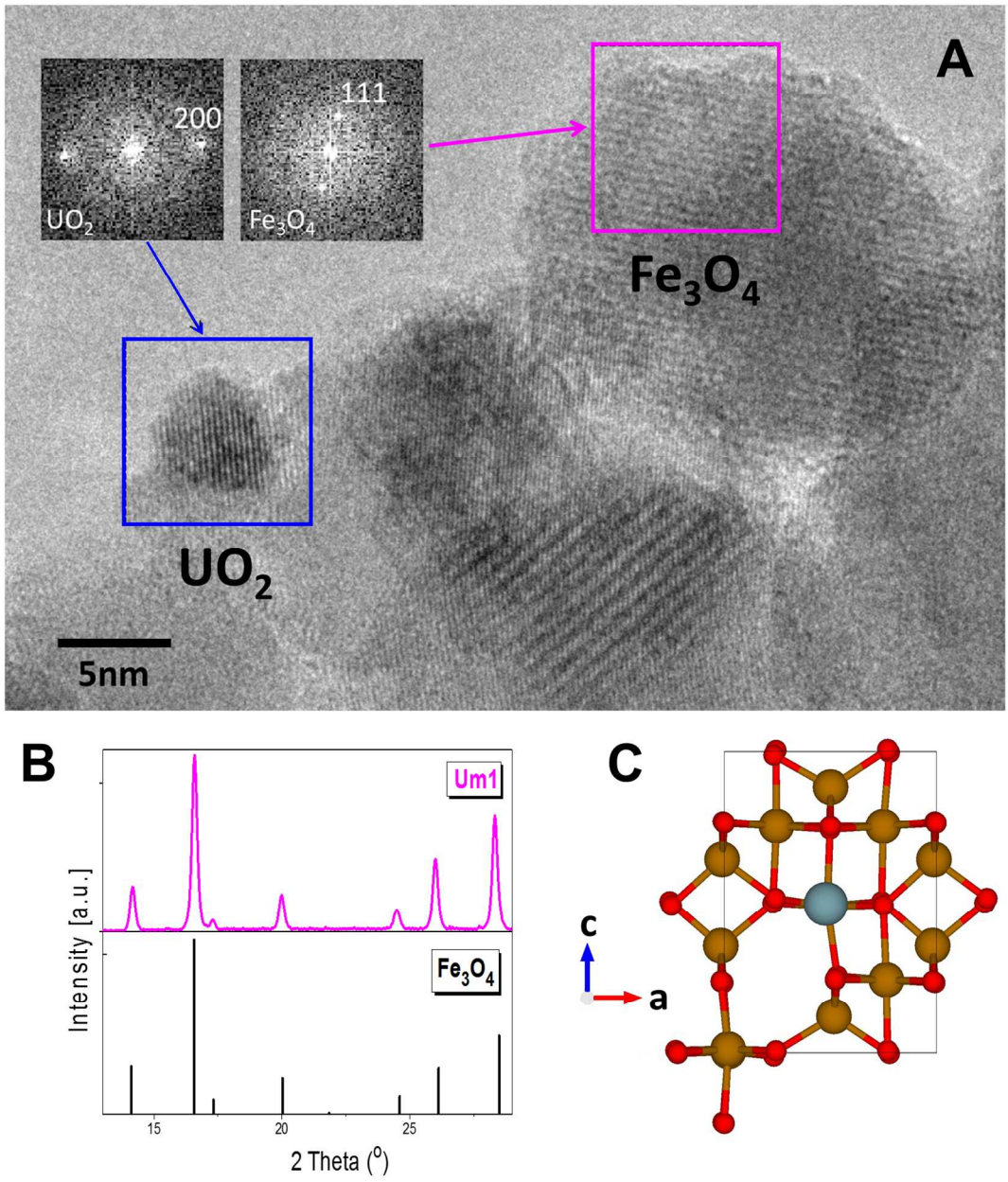

Figure 3. HR-TEM image of UO_2 nanocluster (blue box) and a Fe_3O_4 nanoparticle (magenta box) in the Um1 sample aged for 330 days in anoxic conditions (A). pXRD pattern of the Um1 sample aged for 480 days in anoxic conditions (top) and a reference pXRD pattern of Fe_3O_4 (ICSD 26410) (bottom) (B). U(V) incorporated into an octahedral iron site into the Fe_3O_4 structure as optimized by DFT; O atoms are in red, Fe atoms – brown and U atom – blue (C).

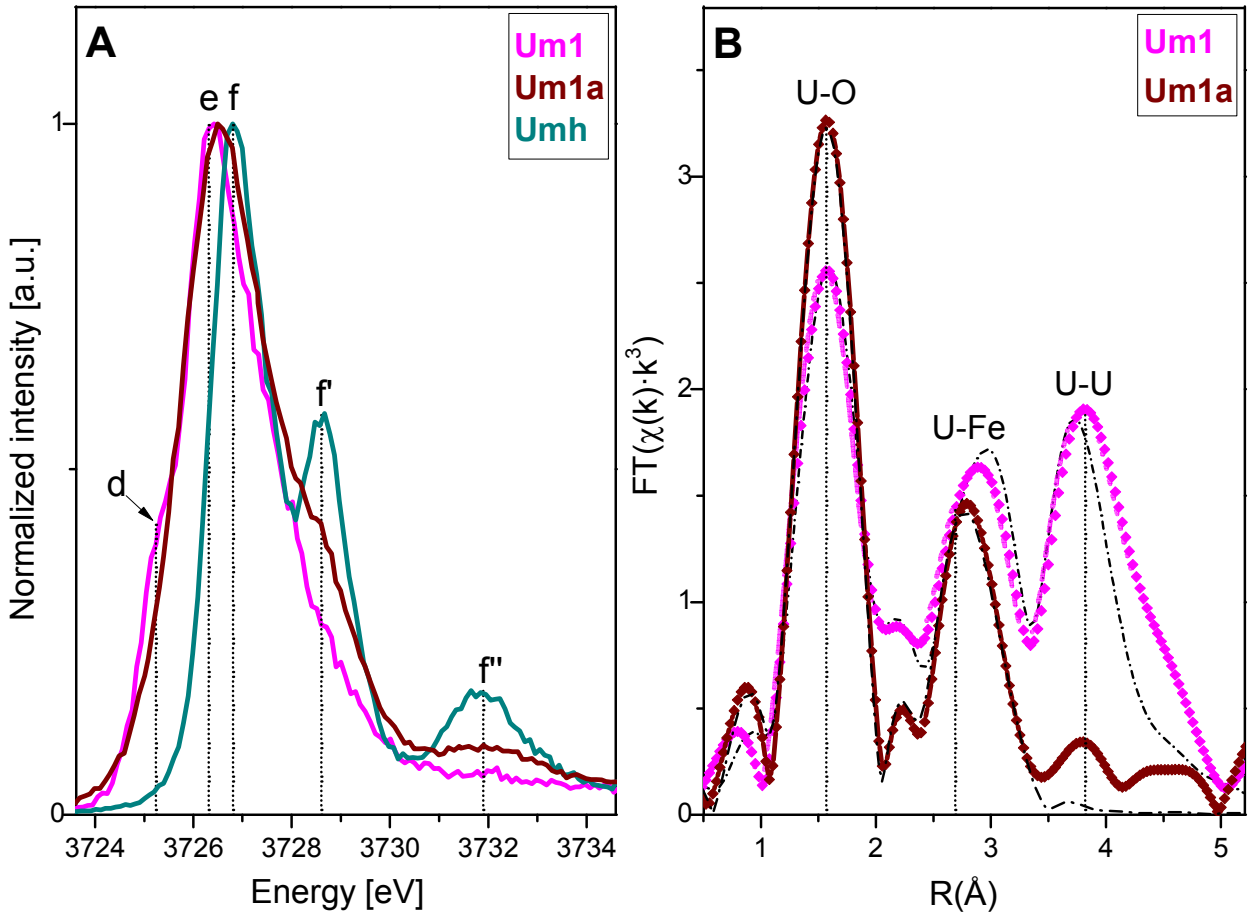

Figure 4. U M_4 HR-XANES spectra of the Um1 and Um1a samples as well as the Umh reference. The Um1 sample was aged for 10 days. The Um1a sample is the Um1 sample aged for 147 days exposed to air for additional 142 days (289 days total ageing time) (A). FT-EXAFS of the Um1 and Um1a samples. The Um1a sample is the Um1 sample aged for 147 days exposed to air for additional 226 days (373 days total ageing time) (B).

ASSOCIATED CONTENT

Supporting Information. Details on the preparation and characterization of the samples, the applied experimental as well as theoretical methods

AUTHOR INFORMATION

Corresponding Author

* tonya.vitova@kit.edu

Present Address

[a] Institute for Nuclear Waste Disposal (INE), Karlsruhe Institute of Technology (KIT), P.O. 3640, D-76021 Karlsruhe, Germany

Funding Sources

This study is funded by the Helmholtz Association of German Research Centres and KIT: Helmholtz Young Investigators Group grant (VH-NG-734).

ACKNOWLEDGMENTS

The authors acknowledge the Helmholtz Association of German Research Centres and KIT for the Helmholtz Young Investigators Group grant (VH-NG-734). We also thank the ESRF and the ANKA synchrotron facilities for the granted beamtime as well as the Radiation Protection officers for the assistance. We thank Philippe Martin (CEA-Marcoule France) for providing the U_4O_9 reference spectrum and Xavier Gaona (INE-KIT) for assistance with the thermodynamic calculations.

REFERENCES

1. Batuk, O. N.; Conradson, S. D.; Aleksandrova, O. N.; Boukhalfa, H.; Burakov, B. E.; Clark, D. L.; Czerwinski, K. R.; Felmy, A. R.; Lezama-Pacheco, J. S.; Kalmykov, S. N.; Moore, D. A.; Myasoedov, B. F.; Reed, D. T.; Reilly, D. D.; Roback, R. C.; Vlasova, I. E.; Webb, S. M.; Wilkerson, M. P., Multiscale Speciation of U and Pu at Chernobyl, Hanford, Los Alamos, McGuire AFB, Mayak, and Rocky Flats. *Environ Sci Technol* **2015,** *49*, (11), 6474-6484.

2. Schlegel, M. L.; Bataillon, C.; Benhamida, K.; Blanc, C.; Menut, D.; Lacour, J. L., Metal corrosion and argillite transformation at the water-saturated, high-temperature iron-clay interface: A microscopic-scale study. *Appl Geochem* **2008,** *23*, (9), 2619-2633.

3. Burns, P. C.; Finch, R. J., Wyartite: Crystallographic evidence for the first pentavalent-uranium mineral. *American Mineralogist* **1999,** *84*, (9), 1456-1460.

4. Dodge, C. J.; Francis, A. J.; Gillow, J. B.; Halada, G. P.; Eng, C.; Clayton, C. R., Association of uranium with iron oxides typically formed on corroding steel surfaces. *Environ Sci Technol* **2002,** *36*, (16), 3504-3511.

5. Duff, M. C.; Coughlin, J. U.; Hunter, D. B., Uranium co-precipitation with iron oxide minerals. *Geochim Cosmochim Ac* **2002,** *66*, (20), 3533-3547.

6. Latta, D. E.; Gorski, C. A.; Boyanov, M. I.; O'Loughlin, E. J.; Kemner, K. M.; Scherer, M. M., Influence of Magnetite Stoichiometry on U-VI Reduction. *Environ Sci Technol* **2012,** *46*, (2), 778-786.

7. O'Loughlin, E. J.; Kelly, S. D.; Cook, R. E.; Csencsits, R.; Kemner, K. M., Reduction of Uranium(VI) by mixed iron(II/iron(III) hydroxide (green rust): Formation of UO2 manoparticies. *Environ Sci Technol* **2003,** *37*, (4), 721-727.

8. O'Loughlin, E. J.; Kelly, S. D.; Kemner, K. M., XAFS Investigation of the Interactions of U-VI with Secondary Mineralization Products from the Bioreduction of Fe-III Oxides. *Environ Sci Technol* **2010,** *44*, (5), 1656-1661.

9. Suzuki, Y.; Kelly, S. D.; Kemner, K. M.; Banfield, J. F., Radionuclide contamination: Nanometre-size products of uranium bioreduction. *Nature* **2002,** *419*, (6903), 134-134.

10. Stewart, B. D.; Neiss, J.; Fendorf, S., Quantifying Constraints Imposed by Calcium and Iron on Bacterial Reduction of Uranium(VI). *Journal of Environmental Quality* **2007,** *36*, (2), 363-372.

11. Boland, D. D.; Collins, R. N.; Payne, T. E.; Waite, T. D., Effect of Amorphous Fe(III) Oxide Transformation on the Fe(II)-Mediated Reduction of U(VI). *Environ Sci Technol* **2011,** *45*, (4), 1327-1333.

12. Ilton, E. S.; Boily, J. F.; Buck, E. C.; Skomurski, F. N.; Rosso, K. M.; Cahill, C. L.; Bargar, J. R.; Felmy, A. R., Influence of Dynamical Conditions on the Reduction of U-VI at the Magnetite-Solution Interface. *Environ Sci Technol* **2010,** *44*, (1), 170-176.

13. Nico, P. S.; Stewart, B. D.; Fendorf, S., Incorporation of Oxidized Uranium into Fe (Hydr)oxides during Fe(II) Catalyzed Remineralization. *Environ Sci Technol* **2009,** *43*, (19), 7391-7396.

14. Ilton, E. S.; Pacheco, J. S. L.; Bargar, J. R.; Shi, Z.; Liu, J.; Kovarik, L.; Engelhard, M. H.; Felmy, A. R., Reduction of U(VI) incorporated in the structure of hematite. *Environmental Science and Technology* **2012,** *46*, (17), 9428-9436.

15. Marshall, T. A.; Morris, K.; Law, G. T. W.; W. Mosselmans, J. F.; Bots, P.; Roberts, H.; Shaw, S., Uranium fate during crystallization of magnetite from ferrihydrite in conditions relevant to the disposal of radioactive waste. *Mineralogical Magazine* **2015,** *79*, (6), 1265-1274.

16. Massey, M. S.; Lezama-Pacheco, J. S.; Jones, M. E.; Ilton, E. S.; Cerrato, J. M.; Bargar, J. R.; Fendorf, S., Competing retention pathways of uranium upon reaction with Fe(II). *Geochim Cosmochim Ac* **2014,** *142*, 166-185.

17. Boland, D. D.; Collins, R. N.; Glover, C. J.; Payne, T. E.; Waite, T. D., Reduction of U(VI) by Fe(II) during the Fe(II)-Accelerated Transformation of Ferrihydrite. *Environ Sci Technol* **2014,** *48*, (16), 9086-9093.

18. Vitova, T.; Kvashnina, K. O.; Nocton, G.; Sukharina, G.; Denecke, M. A.; Butorin, S. M.; Mazzanti, M.; Caciuffo, R.; Soldatov, A.; Behrends, T.; Geckeis, H., High energy resolution x-ray absorption spectroscopy study of uranium in varying valence states. *Phys Rev B* **2010,** *82*, (23), 235118-1-6.

19. Huber, F.; Schild, D.; Vitova, T.; Rothe, J.; Kirsch, R.; Schäfer, T., U(VI) removal kinetics in presence of synthetic magnetite nanoparticles. *Geochim Cosmochim Ac* **2012,** *96*, 154-173.

20. Kvashnina, K. O.; Butorin, S. M.; Martin, P.; Glatzel, P., Chemical State of Complex Uranium Oxides. *Physical Review Letters* **2013,** *111*, (25), 253002.

21. Popa, K.; Prieur, D.; Manara, D.; Naji, M.; Vigier, J.-F.; Martin, P. M.; Dieste Blanco, O.; Scheinost, A. C.; Prumann, T.; Vitova, T.; Raison, P. E.; Somers, J.; Konings, R. J. M., Further

insights into the chemistry of the Bi-U-O system. *Dalton Transactions* **2016,** *45*, (18), 7847-7855.

22. Rothe, J.; Butorin, S.; Dardenne, K.; Denecke, M. A.; Kienzler, B.; Löble, M.; Metz, V.; Seibert, A.; Steppert, M.; Vitova, T.; Walther, C.; Geckeis, H., The INE-Beamline for actinide science at ANKA. *Review of Scientific Instruments* **2012,** *83*, (4), 043105.

23. Vitova, T.; Green, J. C.; Denning, R. G.; Löble, M.; Kvashnina, K.; Kas, J. J.; Jorissen, K.; Rehr, J. J.; Malcherek, T.; Denecke, M. A., Polarization Dependent High Energy Resolution X-ray Absorption Study of Dicesium Uranyl Tetrachloride. *Inorganic Chemistry* **2015,** *54*, (1), 174-182.

24. Walshe, A.; Pru; Vitova, T.; Baker, R. J., An EXAFS and HR-XANES study of the uranyl peroxides [UO2([small eta]2-O2)(H2O)2][middle dot]nH2O (n = 0, 2) and uranyl (oxy)hydroxide [(UO2)4O(OH)6][middle dot]6H2O. *Dalton Transactions* **2014,** *43*, (11), 4400-4407.

25. Rossberg, A.; Reich, T.; Bernhard, G., Complexation of uranium(VI) with protocatechuic acid - application of iterative transformation factor analysis to EXAFS spectroscopy. *Anal Bioanal Chem* **2003,** *376*, (5), 631-638.

26. Baumgartner, J.; Dey, A.; Bomans, P. H. H.; Le Coadou, C.; Fratzl, P.; Sommerdijk, N. A. J. M.; Faivre, D., Nucleation and growth of magnetite from solution. *Nat Mater* **2013,** *12*, (4), 310-314.

27. Jolivet, J. P.; Chaneac, C.; Tronc, E., Iron oxide chemistry. From molecular clusters to extended solid networks. *Chem Commun* **2004**, (5), 481-487.

28. Vayssieres, L.; Chaneac, C.; Tronc, E.; Jolivet, J. P., Size tailoring of magnetite particles formed by aqueous precipitation: An example of thermodynamic stability of nanometric oxide particles. *J Colloid Interf Sci* **1998,** *205*, (2), 205-212.

29. Kvashnina, K. O.; Kvashnin, Y. O.; Butorin, S. M., Role of resonant inelastic X-ray scattering in high-resolution core-level spectroscopy of actinide materials. *Journal of Electron Spectroscopy and Related Phenomena* **2014,** *194*, 27-36.

30. Cornell, R. M.; Schwertmann, U., *The Iron Oxides: Structure, Properties, Reactions, Occurrences and Uses*. Wiley: 2006.

31. Gauthier, C.; Sole, V. A.; Signorato, R.; Goulon, J.; Moguiline, E., The ESRF beamline ID26: X-ray absorption on ultra dilute sample. *J Synchrotron Radiat* **1999,** *6*, 164-166.

32. Glatzel, P.; Bergmann, U., High resolution 1s core hole X-ray spectroscopy in 3d transition metal complexes—electronic and structural information. *Coordination Chemistry Reviews* **2005,** *249*, (1–2), 65-95.

33. Kvashnina, K. O.; Scheinost, A. C., A Johann-type X-ray emission spectrometer at the Rossendorf beamline. *J Synchrotron Radiat* **2016,** *23*, (3), 836-841.

34. Ankudinov, A. L.; Ravel, B.; Rehr, J. J.; Conradson, S. D., Real-space multiple-scattering calculation and interpretation of x-ray-absorption near-edge structure. *Phys Rev B* **1998,** *58*, (12), 7565-7576.

35. Ravel, B.; Newville, M., ATHENA, ARTEMIS, HEPHAESTUS: data analysis for X-ray absorption spectroscopy using IFEFFIT. *J Synchrotron Radiat* **2005,** *12*, (4), 537-541.

36. Goettlicher, J.; Kotelnikov, A.; Suk, N.; Kovalski, A.; Vitova, T.; Steininger, R., Sulfur K X-ray absorption near edge structure spectroscopy on the photochrome sodalite variety hackmanite. *Z Kristallogr* **2013,** *228*, (3), 157-171.

37. Hammersley, A. P.; Svensson, S. O.; Hanfland, M.; Fitch, A. N.; Häusermann, D., Two-dimensional detector software: From real detector to idealised image or two-theta scan. *High Pressure Research* **1996,** *14*, (4-5), 235-248.

38. Kresse, G.; Furthmuller, J., Efficient iterative schemes for ab initio total-energy calculations using a plane-wave basis set. *Phys Rev B* **1996,** *54*, (16), 11169-11186.

39. Kresse, G.; Furthmuller, J., Efficiency of ab-initio total energy calculations for metals and semiconductors using a plane-wave basis set. *Comp Mater Sci* **1996,** *6*, (1), 15-50.

40. Kresse, G.; Hafner, J., Ab-Initio Molecular-Dynamics for Open-Shell Transition-Metals. *Phys Rev B* **1993,** *48*, (17), 13115-13118.

41. Perdew, J. P.; Burke, K.; Ernzerhof, M., Generalized gradient approximation made simple. *Physical Review Letters* **1996,** *77*, (18), 3865-3868.

42. Blochl, P. E., Projector Augmented-Wave Method. *Phys Rev B* **1994,** *50*, (24), 17953-17979.

43. Kresse, G.; Joubert, D., From ultrasoft pseudopotentials to the projector augmented-wave method. *Phys Rev B* **1999,** *59*, (3), 1758-1775.

44. Rollmann, G.; Rohrbach, A.; Entel, P.; Hafner, J., First-principles calculation of the structure and magnetic phases of hematite. *Phys Rev B* **2004,** *69*, (16), 165107-1-12.

45. Puigdomènech, I.; Colàs, E.; Grivé, M.; Campos, I.; García, D. In *A tool to draw chemical equilibrium diagrams using SIT: Applications to geochemical systems and radionuclide solubility*, Materials Research Society Symposium Proceedings, 2014; 2014; pp 111-116.

46. Soldatov, A. V.; Lamoen, D.; Konstantinović, M. J.; Van den Berghe, S.; Scheinost, A. C.; Verwerft, M., Local structure and oxidation state of uranium in some ternary oxides: X-ray absorption analysis. *Journal of Solid State Chemistry* **2007,** *180*, (1), 54-61.

47. Kosog, B.; La Pierre, H. S.; Denecke, M. A.; Heinemann, F. W.; Meyert, K., Oxidation State Delineation via U L-III-Edge XANES in a Series of Isostructural Uranium Coordination Complexes. *Inorganic Chemistry* **2012,** *51*, (14), 7940-7944.

48. Podkovyrina, Y.; Pidchenko, I.; Prüßmann, T.; Bahl, S.; Göttlicher, J.; Soldatov, A.; Vitova, T., Probing Covalency in the UO 3 Polymorphs by U M 4 edge HR- XANES. *Journal of Physics: Conference Series* **2016,** *712*, (1), 012092.

49. Pidchenko, I.; Green, J. C.; Fellhauer, D.; Bahl, S.; Prüßmann, T.; Bohnert, E.; Rothe, J.; Geckeis, H.; Vitova, T., Decrease of covalency in UO_2^+. In preparation.

50. Nelin, C. J.; Bagus, P. S.; Ilton, E. S., Theoretical analysis of the U L<inf>3</inf>-edge NEXAFS in U oxides. *RSC Advances* **2014,** *4*, (14), 7148-7153.

51. Van den Berghe, S.; Verwerft, M.; Laval, J. P.; Gaudreau, B.; Allen, P. G.; Van Wyngarden, A., The Local Uranium Environment in Cesium Uranates: A Combined XPS, XAS, XRD, and Neutron Diffraction Analysis. *Journal of Solid State Chemistry* **2002,** *166*, (2), 320-329.

52. Bès, R.; Rivenet, M.; Solari, P. L.; Kvashnina, K. O.; Scheinost, A. C.; Martin, P. M., Use of HERFD-XANES at the U L3- and M4-Edges to Determine the Uranium Valence State on [Ni(H2O)4]3[U(OH,H2O)(UO2)8O12(OH)3]. *Inorganic Chemistry* **2016,** *55*, (9), 4260-4270.

53. Pidchenko, I.; Heberling, F.; Kvashnina, K. O.; Finck, N.; Schild, D.; Bohnert, E.; Schäfer, T.; Rothe, J.; Geckeis, H.; Vitova, T., Aqueous U(VI) interaction with magnetite nanoparticles in a mixed flow reactor system: HR-XANES study. *Journal of Physics: Conference Series* **2016,** *712*, (1), 012086.

54. Latta, D. E.; Mishra, B.; Cook, R. E.; Kemner, K. M.; Boyanov, M. I., Stable U(IV) Complexes Form at High-Affinity Mineral Surface Sites. *Environ Sci Technol* **2014,** *48*, (3), 1683-1691.

55. Conradson, S. D.; Manara, D.; Wastin, F.; Clark, D. L.; Lander, G. H.; Morales, L. A.; Rebizant, J.; Rondinella, V. V., Local structure and charge distribution in the UO2-U4O9 system. *Inorganic Chemistry* **2004,** *43*, (22), 6922-6935.

56. Debets, P. C., Structure of Beta-Uo3. *Acta Crystallogr* **1966,** *21*, 589-&.

57. Kerisit, S.; Felmy, A. R.; Ilton, E. S., Atomistic Simulations of Uranium Incorporation into Iron (Hydr)Oxides. *Environ Sci Technol* **2011,** *45*, (7), 2770-2776.

58. Ilton, E. S.; Haiduc, A.; Cahill, C. L.; Felmy, A. R., Mica surfaces stabilize pentavalent uranium. *Inorganic Chemistry* **2005,** *44*, (9), 2986-2988.

59. Belai, N.; Frisch, M.; Ilton, E. S.; Ravel, B.; Cahill, C. L., Pentavalent Uranium Oxide via Reduction of [UO2](2+) Under Hydrothermal Reaction Conditions. *Inorganic Chemistry* **2008,** *47*, (21), 10135-10140.

60. Singer, D. M.; Chatman, S. M.; Ilton, E. S.; Rosso, K. M.; Banfield, J. F.; Waychunas, G. A., Identification of Simultaneous U(VI) Sorption Complexes and U(IV) Nanoprecipitates on the Magnetite (111) Surface. *Environ Sci Technol* **2012,** *46*, (7), 3811-3820.

61. Payne, T. E. L., G.R.; Waite, T.D. , Uranium(VI) sorption on model minerals. In *Sorption of Metals by Geomedia*, Jenne, E. A., Ed. 1998; pp 75-97.

Table of Contents Graphic.